Discrete vector solitons in one-dimensional lattices in photorefractive media

E. P. Fitrakis,[1] P. G. Kevrekidis,[2] B. A. Malomed,[3] and D. J. Frantzeskakis[1]
[1]*Department of Physics, University of Athens, Panepistimiopolis, Zografou, Athens 15784, Greece*
[2]*Department of Mathematics and Statistics, University of Massachusetts, Amherst, Massachusetts 01003-4515, USA*
[3]*Department of Interdisciplinary Studies, Faculty of Engineering, Tel Aviv University, Tel Aviv 69978, Israel*
(Received 8 March 2006; published 18 August 2006)

We construct families of two-component spatial solitons in a one-dimensional lattice with saturable on-site nonlinearity (focusing or defocusing) in a photorefractive crystal. We identify 14 species of vector solitons, depending on their type (bright/dark), phase (in-phase/staggered), and location on the lattice (on/off-site). Two species of the bright/bright type form *entirely stable* soliton families, four species are partially stable (depending on the value of the propagation constant), while the remaining eight species are completely unstable. "Symbiotic" soliton pairs (of the bright/dark type), which contain components that cannot exist in isolation in the same model, are found as well.

DOI: 10.1103/PhysRevE.74.026605 PACS number(s): 42.65.Tg, 42.70.Nq, 05.45.Yv

I. INTRODUCTION

In the past few years, quasidiscrete spatial solitons were observed experimentally in planar materials with etched waveguide arrays [1,2] and in photorefractive crystals with light-induced lattices [3]. The demonstrated lattice solitons were bright and dark (the latter were proposed in Ref. [4]), both of the in-phase and the staggered type. In the staggered case, waves propagating in adjacent waveguides are π out-of-phase with each other [5]. Photorefractive crystals are often used for the realization of such quasidiscrete patterns (see, e.g., recent reviews in [6,7]) because they offer real-time control of the waveguide array, as well as strong and tunable nonlinearity [8]. Discrete spatial solitons are supported in such systems by the balance of the on-site nonlinearity and discrete diffraction. Since the discrete optical solitons were predicted [9], many applications have been proposed for them, such as photonic switching [10]. In view of the above, two-component (alias vectorial) discrete solitons may be especially promising, as the structure of the signal component may be affected by the control beam (see, e.g., [11] for an overview and [12,13] for relevant experimental observations).

In this work, we study the stability and propagation dynamics of two-component discrete spatial solitons with saturable on-site nonlinearity, corresponding to an array of photorefractive waveguides; single-component discrete solitons supported by the nonlinearity of this type were recently studied in Refs. [14,15] and their collisions were also examined [16]. Soliton pairs of the bright–bright and dark–bright types will be considered here. In a scaled form, the model is based on the following coupled discrete equations of the so-called Vinetskii-Kukhtarev model (without the diffusion term) [17–19]:

$$i\frac{\partial \psi_{1,n}}{\partial z} + \alpha_1(\psi_{1,n+1} + \psi_{1,n-1} - 2\psi_{1,n}) - \frac{\beta_1(1+\rho)}{1+|\psi_{1,n}|^2+|\psi_{2,n}|^2}\psi_{1,n} = 0, \tag{1}$$

$$i\frac{\partial \psi_{2,n}}{\partial z} + \alpha_2(\psi_{2,n+1} + \psi_{2,n-1} - 2\psi_{2,n}) - \frac{\beta_2(1+\rho)}{1+|\psi_{1,n}|^2+|\psi_{2,n}|^2}\psi_{2,n} = 0, \tag{2}$$

where n is the lattice site number, discrete fields $\psi_{(1,2),n}$ are measured in units of $n_e^{-1/2}(2\sqrt{\mu_0/\epsilon_0}I_d)^{1/2}$, with I_d being the dark irradiance of the crystal, while the propagation distance z is normalized to kx_0^2, where $k=2\pi n_e/\lambda$ is the wave number of the beam in the crystal (λ is the wavelength and n_e is the extraordinary refractive index of the crystal), and x_0 is the spacing between adjacent guiding cores. Furthermore, $\alpha_{1,2}$ are normalized diffraction coefficients, and $\rho=I_\infty/I_d$, where I_∞ is the total power density of the light signal far from the center of the crystal, in the case when the soliton contains a dark component. The signs of the nonlinearity coefficients $\beta_{1,2}$ depend on the polarity of the applied voltage. Equations (1) and (2) conserve three dynamical invariants: the Hamiltonian,

$$H = \sum_n \sum_{j=1,2} \frac{\alpha_j}{\beta_j}|\psi_{n+1}-\psi_n|^2 + (1+\rho)\ln(1+|\psi_{1,n}|^2+|\psi_{2,n}|^2),$$

and two norms, $P_j=\Sigma_n|\psi_{j,n}|^2$. Below, we will characterize the solutions by the total norm,

$$P \equiv P_1 + P_2. \tag{3}$$

The model implies that the two soliton-forming beams in the extraordinary polarization are mutually incoherent, so that they interact solely through the cross-phase modulation (XPM). This can be achieved by using signals carried by different frequencies, which implies, generally speaking, $\alpha_1 \neq \alpha_2$ and $\beta_1 \neq \beta_2$ in Eqs. (1) and (2). Another option is to use a laser source with an appropriate coherence length and vary the optical paths of the two signal beams before entering the crystal. In the latter case, one has $\alpha_1=\alpha_2$ and $\beta_1=\beta_2$. In this work we focus on this second case.

The system's discreteness is induced by use of two ordinarily polarized plane waves that form the waveguiding pattern (photonic lattice) through the holographic method (see, e.g., Ref. [20]). This pattern extends undistorted along the z axis, as the crystal is practically a linear medium for the ordinary polarization. Two probe beams that support the two-component solitary wave structure are launched in the extraordinary polarization, for which the anisotropic photorefractive crystal features strong nonlinearity. This setup creates a 1D environment for the experiment.

We look for stationary solutions to Eqs. (1) and (2) in the usual form,

$$\psi_{j,n} = \exp(i\Lambda_j z)u_{j,n}, \quad j = 1,2. \tag{4}$$

Solutions of the boundary-value problem obtained by the substitution of Eq. (4) in Eqs. (1) and (2) are found, by means of the Newton-Raphson root-finding algorithm, as fixed points of a numerical iteration scheme on the lattice grid. Having found the stationary solutions, the linear stability analysis is performed by assuming a weakly perturbed solution (see, e.g., [21]),

$$\psi_{1,n}(z) = \exp(i\Lambda_1 z)\{u_{1,n} + \epsilon[a_n \exp(-\xi z) + b_n \exp(-\xi^* z)]\}, \tag{5}$$

$$\psi_{2,n}(z) = \exp(i\Lambda_2 z)\{u_{2,n} + \epsilon[c_n \exp(-\xi z) + d_n \exp(-\xi^* z)]\}, \tag{6}$$

where ϵ is the amplitude of infinitesimal perturbations, and ξ is a (generally complex) eigenvalue (the asterisk stands for the complex conjugation), which is to be found from the linearization of Eqs. (1) and (2) along with the corresponding eigenfunctions a_n, b_n and c_n, d_n. In the computations, Dirichlet boundary conditions are used with a grid of a size sufficiently large to ensure that boundary effects do not affect the results.

Taking equal propagation constants in Eq. (4), $\Lambda_1 = \Lambda_2 \equiv \Lambda$, we will find *asymmetric* two-component solutions, even when both components are of the same type [for instance, bright unstaggered on-site-centered, see Fig. 1(a) below]. Such asymmetric solutions, of the form $\psi_1 = C\,\psi_2$ (where C is a constant), are expected for equal diffraction coefficients (and equal nonlinearilty coefficients). If $\alpha_1 \neq \alpha_2$, asymmetric solutions can still be obtained from symmetric ones by other trivial scalings.

A summary of types of compound solitons ("soliton pairs") that we will consider in this work is presented in Table I. In total, six pairs turned out to be fully or partially stable. It is interesting to note the possibility of finding "symbiotic" solitons, which contain stable components that cannot exist as single-component solitons in the same model (the notion of two-component symbiotic solitons, which contain components that cannot exist in isolation, was elaborated, in various contexts, related to nonlinear optics and Bose-Einstein condensation, in Ref. [22]). For example, the unstaggered bright soliton normally needs self-focusing nonlinearity, but, as will be shown in Sec. II, it can exist in the self-defocusing regime, as a part of an on-site dark–bright soliton pair.

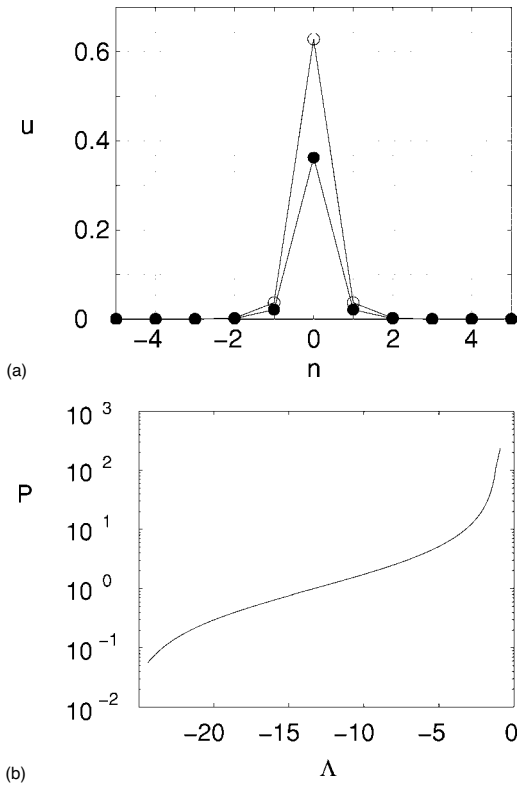

FIG. 1. (a) An example of a numerically found stable stationary solution of Eqs. (1) and (2) for the on-site bright–bright soliton pair, with $\beta = 24.7$ and $\Lambda_1 = \Lambda_2 = -17.1$. Note that the two components of the soliton, shown by empty and filled circles, have different amplitudes, although they pertain to equal propagation constants. (b) A family of stable asymmetric bright-bright unstaggered on-site-centered solitons, shown in terms of the total power vs the common propagation constant (on the semilogarithmic scale), with $\beta = 24.7$ and $\Lambda_1 = \Lambda_2 \equiv \Lambda$.

II. RESULTS

To solve Eqs. (1) and (2) numerically, we take values of parameters relevant to the experiment (in particular, to the experimental setup used in Ref. [3], with a SBN:75 crystal), $\alpha_1 = \alpha_2 \equiv \alpha = 0.5$, and $\beta_1 = \beta_2 \equiv \beta = (1/2)k_0^2 x_0^2 n_e^4 r_{33} E_0$, with $r_{33} = 1340$ pm/V, E_0 being the dominant screening nonlinearity, measured in V/mm, which can be tuned by the applied dc bias field. A wavelength of 0.5 μm is assumed for both components of the signal, and the spacing x_0 is set to be 10 μm. Accordingly, the normalization defined above implies that the lattice spacing, which is set to be 1 in Eqs. (1) and (2), corresponds to the physical length of 10 μm in the transverse direction, while a normalized length of 3.4 in the propagation direction (z) corresponds to the physical distance of 1 cm.

The Newton-Raphson algorithm was initialized with the following profiles for the bright and dark components:

$$u_{\text{bright}} = A_b \,\text{sech}\left(\frac{n - s_1/2}{w_b}\right)\cos(s_2 \pi n), \tag{7}$$

TABLE I. Summary of numerical results for the pairs that were tested as vector-soliton solutions to Eqs. (1) and (2). Initial guesses for the Newton-Raphson (NR) root-finding algorithm were taken as per Eqs. (7) and (8). The stability of the solutions was analyzed through linear-stability analysis and then tested in direct simulations by numerical time-integration, using a fourth-order Runge-Kutta algorithm.

	On-site		Off-site	
Type	Stability	Instability	Stability	Instability
Bright–bright	Stable		Unstable	Evolves into on-site
Bright–staggered-bright	Unstable	Evolves into bright–bright	Unstable	Decays
Staggered-bright–staggered-bright	Stable		Partially stable	Decays
Dark–bright	Partially stable	Decays	Unstable	Decays
Dark–staggered-bright	Unstable	Decays	Unstable	Decays
Staggered-dark–bright	Partially stable	Decays	Unstable	Decays
Staggered-dark–staggered-bright	Partially stable	Decays	Unstable	Evolves into on-site

$$u_{\text{dark}} = A_d \tanh\left(\frac{n - s_1/2}{w_d}\right)\cos(s_2 \pi n), \tag{8}$$

where s_1 is 0 or 1 for on- and off-site-centered solitons, respectively, while s_2 is 0 and 1 for in-phase (unstaggered) and staggered configurations. Note that the staggered off-site expression (7) can be cast in the form

$$u_{\text{bright}} = -A_b \,\text{sech}\left(\frac{\nu}{w_b}\right)\sin(s_2 \pi \nu), \quad \nu \equiv n - 1/2, \tag{9}$$

which is *odd* with respect to the central point, $\nu=0$. We initialize our numerical guesses of Eqs. (7)–(9) above using $w_{b1}=w_{b2}=0.3$ and $w_d=w_b=0.5$ for the pairs including two bright components or a combination of dark and bright ones, respectively.

A necessary condition for the stability of the bright–bright vector soliton, when only unstaggered components are involved, is that the bias (i.e., the sign of the parameter β) is positive. On the other hand, when the components are staggered ones, negative bias is required for the stability. As the bright–bright pair with mixed components (i.e., bright–staggered-bright) is found to be unstable, one can conclude the following: Stability of a bright–bright vector soliton requires the sign of the bias to be the one that can support each component in the uncoupled system. On the other hand, the stability of dark–bright vector solitons is directly connected to the stability of the background of the dark component; the latter is necessary, as, in the case of an unstable pedestal, the respective vector soliton solution has no physical purport. Hence the sign of the bias has to be negative when the dark component is unstaggered, and positive when it is staggered. This requirement also applies to the cases where the amplitude of the bright component is greater than that of the dark one (this has been checked by direct simulations).

A. Stable soliton pairs

1. On-site bright–bright soliton pair

Adjusting parameters to the real experiment [3,8], we took two different amplitudes, $A_b^{(1)}=0.5\sqrt{3}$ and $A_b^{(2)}=0.5$, in initial guesses (7) for two bright components. Recall that these amplitudes are normalized with respect to the dark irradiance of the crystal (which is externally tunable); typically, this value is on the order of mWs or tens of mWs in physical units. As mentioned above, the sign of the bias has to be such that it can support each component in the uncoupled system; since an unstaggered bright soliton is supported by self-focusing nonlinearity, the bias here is taken to be positive, $\beta>0$.

With $\beta=24.7$ and $\Lambda_1=\Lambda_2=-17.1$ in Eq. (4), the algorithm converges to a stationary state. This example of the vector soliton is displayed in Fig. 1(a). Note that, starting with *unequal* amplitudes of the two components of the same type (bright unstaggered on-site-centered), the solution converges to the *asymmetric* shape, even though the components appertain to equal propagation constants. The stability of the vector soliton was established by means of the linear-stability analysis, and verified in direct simulations (with the Runge-Kutta method), for propagation distances that are three orders of magnitude greater than those relevant to current experiments (the latter is a few mm). The same check has been performed for all stable solitons reported in this paper.

Further, fixing $\beta=24.7$ and varying $\Lambda_1=\Lambda_2\equiv\Lambda$, we present the results for the family of the *asymmetric* on-site bright–bright pairs in Fig. 1(b), as the total norm (3) vs Λ, with a step of $\Delta\Lambda=0.1$ (the computation was restricted to 21 sites of the grid). The entire family is stable.

2. On-site staggered-bright–staggered-bright soliton pair

In this case, we used the initial configuration (7) with the same (unequal) amplitudes of the two components as above, $A_b^{(1)}=0.5\sqrt{3}$ and $A_b^{(2)}=0.5$; additionally, we assumed *negative* bias, $\beta<0$. An example of a stable *asymmetric* solution of this type is shown in Fig. 2(a). Then, fixing the same $\beta=-24.7$, and varying $\Lambda_1=\Lambda_2=\Lambda$, we plot the continuation diagram for the family of these asymmetric solutions, $P(\Lambda)$, in Fig. 2(b).

B. Partially stable soliton pairs

The soliton pairs in this section build families that have both stable and unstable parts. In their unstable regime, the pairs decay.

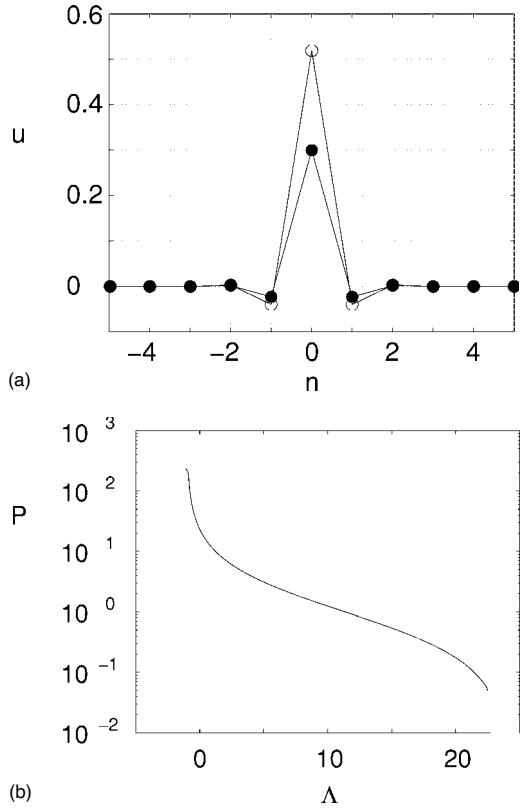

FIG. 2. (a) A numerically found stationary asymmetric solution of Eqs. (1) and (2) for a stable soliton pair of the on-site staggered-bright–staggered-bright type, with $\beta=-24.7$, $\Lambda_1=\Lambda_2=17.1$. (b) The continuation diagram for the family of vector solitons of the same type, with $\beta=-24.7$ and $\Lambda_1=\Lambda_2\equiv\Lambda$. The entire family is stable.

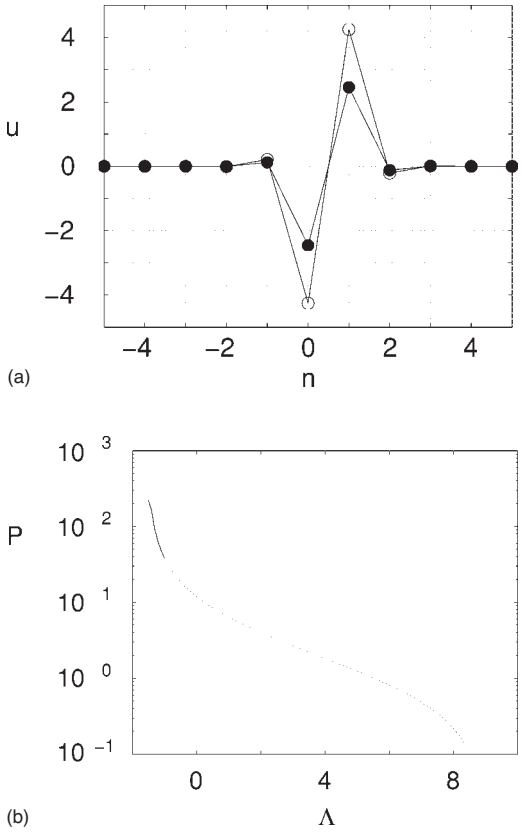

FIG. 3. (a) A numerically found stationary solution of Eqs. (1) and (2) for a stable asymmetric off-site staggered-bright–staggered-bright soliton pair, with $\beta=-10.7$ and $\Lambda_1=\Lambda_2=-1.1$. The shape of each component is odd. (b) The continuation diagram for a family of soliton pairs of the same type, for $\beta=-10.7$ and $\Lambda_1=\Lambda_2\equiv\Lambda$. Solid and dotted parts of the plot depict stable and unstable parts of the family.

1. Off-site staggered-bright–staggered-bright soliton pair

The vector soliton of this type was sought for starting with the staggered off-site-centered configuration (7) that had $A_b^{(1)}=\sqrt{3}$, $A_b^{(2)}=1$, and $\beta<0$ (negative bias). An example of a stable asymmetric solution is shown in Fig. 3(a). Note that, in accordance with Eq. (9), this soliton is odd, with respect to the central point.

A continuous family of the solutions is displayed, in terms of the $P(\Lambda)$ plot, in Fig. 3(b) for fixed bias, $\beta=-10.7$. As seen in the figure, only a small part of this family is stable, in sharp contrast with its on-site counterpart, which was shown above to be entirely stable.

2. On-site dark–bright soliton pair

Proceeding to soliton pairs with a dark component, we used the initial configurations (7) and (8) with $A_d=A_b=0.6$. In the case of dark–bright pairs, it is reminded that the nonlinearity has to be of the sign that can support the background of the dark component in the uncoupled system. Therefore, in the case under consideration, the nonlinearity has to be self-defocusing, $\beta<0$, so that the unstaggered dark component's pedestal is stable. Note that the required sign of the bias is negative, even when the amplitude of the bright component is greater than that of the dark one (we will not consider such cases here).

An example of the stable state, and a family of the solutions, which includes stable and unstable segments, are shown in Figs. 4(a) and 4(b). The family is generated by fixing $\beta=-15.6$ and $\Lambda_d=15.6$, while the propagation constant of the bright component varies, generating the family in the interval $15.7<\Lambda_b<23.7$. At $\Lambda_b=15.6$, the Newton-Raphson numerical algorithm ceases to converge, while at $\Lambda_b=23.7$ the solution disappears, as its amplitude drops below 10^{-3}. We stress that, with the self-defocusing nonlinearity, an unstaggered bright soliton cannot exist in isolation; however, in the present setting, it is supported, and may be made stable, by pairing to the dark component to form a "symbiotic" soliton pair. A similar result is known in the continuous photorefractive medium [23].

3. On-site staggered-dark–bright soliton pair

A stable solution of this type was found, for instance, for $\Lambda_b=-21.7$ and $\Lambda_d=-16.1$, and initial amplitudes $A_b=A_d=0.6$, taking positive bias, $\beta=14.1$, see Fig. 5(a). Depending on values of Λ_b and Λ_d, the initial ansatz may also generate a stable on-site pair in which a staggered-dark component is paired to a *staggered* bright soliton, unlike the unstaggered bright component in Fig. 5(a).

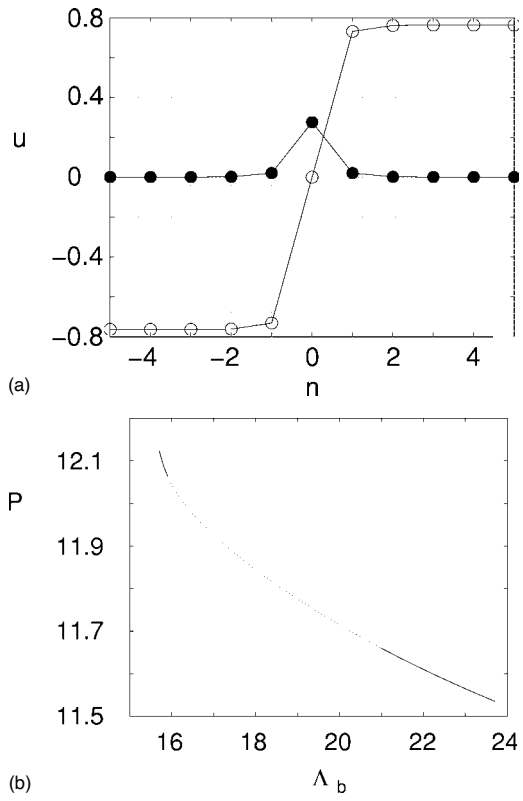

FIG. 4. (a) A numerically found stationary solution of Eqs. (1) and (2) in the form of a stable on-site-centered dark–bright soliton pair, for $\beta=-15.6, \Lambda_d=15.6$, and $\Lambda_b=22$. Linear stability analysis has shown this pair to be stable. (b) The continuation diagram for the family of soliton pairs of the same type, for fixed $\beta=-15.6$ and $\Lambda_d=15.6$, and varying Λ_b. Stable parts of the family are depicted by solid lines.

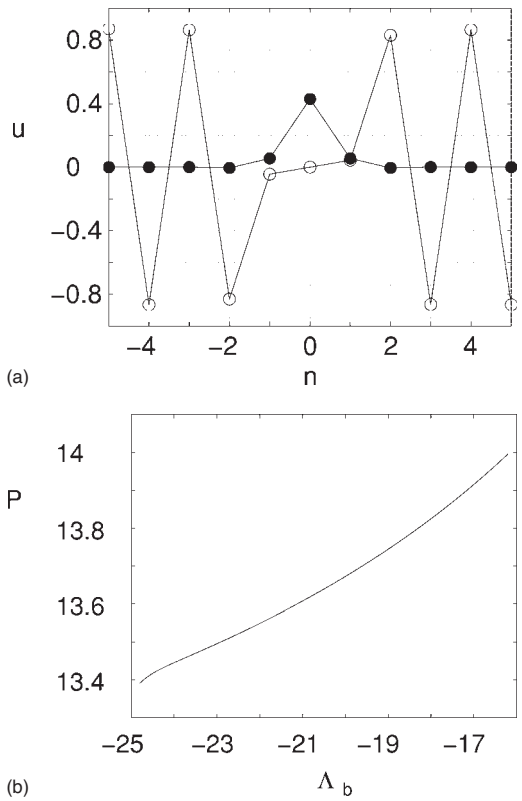

FIG. 5. (a) Numerical solution of Eqs. (1) and (2) for a stable soliton pair of the on-site-centered staggered-dark–bright type, for $\beta=14.1$, $\Lambda_b=-21.7$, and $\Lambda_d=-16.1$. (b) The continuation diagram for the family of vector solitons of the same type, for $\beta=14.1$ and $\Lambda_d=-16.1$. Although this plot is shown by a solid line, detailed analysis demonstrates that it actually contains many small stability and instability regions.

Fixing $\beta=14.1$, $\Lambda_d=-16.1$, and changing Λ_b, we have drawn the continuation diagram, in the form of $P(\Lambda_b)$, as shown in Fig. 5(b). This family of the vector solitons is found in the interval of $-24.9<-\Lambda_b<-16.2$. At the right edge of the interval, the Newton-Raphson algorithm ceases to converge, while at the left edge the bright-soliton component of the solution disappears, as its amplitude drops below 10^{-3}. Note that, although this plot is shown by a solid line, detailed analysis demonstrates that it actually contains many small stability and instability regions.

4. On-site staggered-dark–staggered-bright soliton pair

An example of a stable soliton pair of this type is shown in Fig. 6(a), for $\Lambda_b=-22.7$ and $\Lambda_d=-17.3$, and positive bias, with $\beta=15.3$. The solution was generated by the initial ansatz (7) and (8) with the amplitudes $A_b=A_d=0.6$.

Fixing $\beta=15.3$, $\Lambda_d=-17.3$, and varying Λ_b, we have drawn the continuation diagram, $P(\Lambda_b)$, in Fig. 6(b). The family of the vector solitons displayed in this figure is found in the interval of $-25.7<\Lambda_2<-17.5$. Again, the numerical algorithm stops converging at the right edge of the interval, and the bright component disappears at the left edge, dropping below the level of 10^{-3}.

Staggered bright solitons cannot exist, by themselves, in the model with self-focusing. However, stable vector solitons, such as the one shown in Fig. 6(a), may contain a component of this type in the self-focusing regime, because it is supported and stabilized by coupling with the staggered-dark component. This is another example of a potentially stable "symbiotic" soliton.

C. Unstable pairs

We have constructed eight more species of discrete soliton pairs, that, however, lead to entirely unstable families of vector solitons. As shown in Table I, these unstable species involve on-site bright–staggered-bright and dark–staggered-bright pairs, as well as pairs of the off-site bright–bright, bright–staggered-bright, dark–bright, dark–staggered-bright, staggered-dark–bright, and staggered-dark–staggered-bright types. In direct numerical simulations, most of these pairs decay, with the exception of three species, the dynamics of which is briefly described below.

The vector solitons of the off-site-centered bright–bright and the off-site staggered-dark–staggered-bright types do not decay, but rather spontaneously reshape into their counterparts which are centered on-site. In particular, in the model with positive bias (self-focusing nonlinearity) the unstable

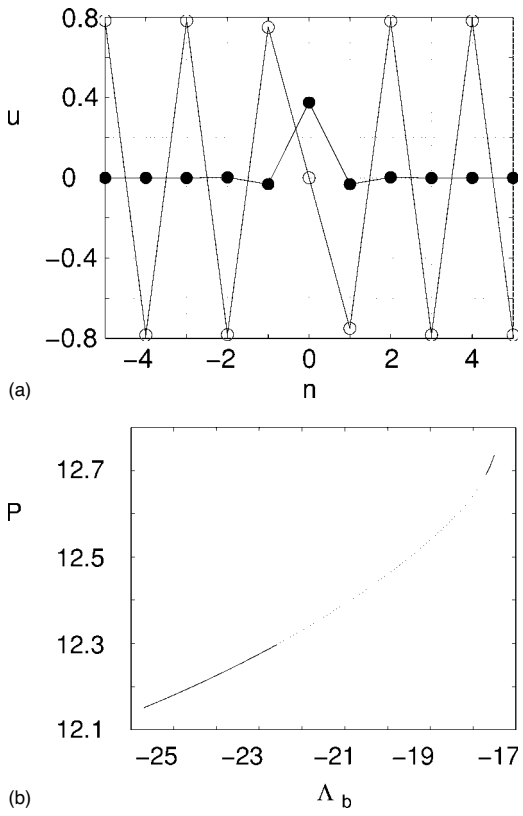

FIG. 6. (a) Numerical solution of Eqs. (1) and (2) for a stable on-site-centered soliton pair of the staggered-dark–staggered-bright type, for $\beta=15.3$ and $\Lambda_d=-17.3$, $\Lambda_b=-22.7$. (b) Continuation diagram for the family of vector solitons of this type, with $\beta=15.3$ and $\Lambda_d=-17.3$ kept constant. Regions of stable solutions are drawn by the solid line.

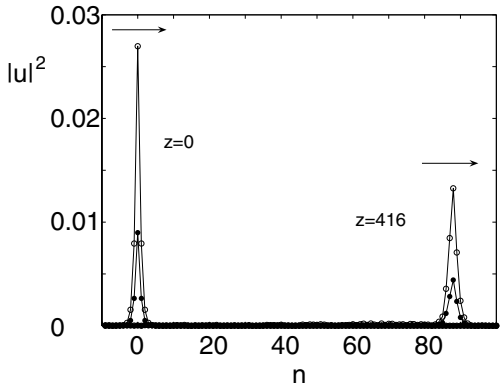

FIG. 7. Illustration of the on-site bright–bright vector soliton dynamics, when the stationary solution (generated with the Newton-Raphson method) is multiplied by a transverse-momentum factor $\exp(imn)$ and then introduced into the propagation algorithm. In this case the vector soliton moves across the lattice (transverse dimension) while propagating along z (perpendicular to the page). The initial condition of the vector pair is shown at $z=0$, located at $n=0$, while a later snapshot is shown at $z=416$ (≈ 1.22 m in physical units), located at $n=88$ (0.88 mm to the right, in physical units). Each soliton component has already lost $\approx 50\%$ of its peak density at $z=35$, but then stabilizes at these values. The parameters in this example are $\Lambda_1=\Lambda_2=-23.9$, $\beta=24.7$, and $m=0.3\pi$.

off-site bright–bright pair evolves into a vector soliton of the on-site bright–bright type. In addition to these two unstable species, the on-site bright–staggered-bright pair spontaneously transforms into its stable counterpart of the on-site bright–bright type.

D. Moving vector solitons

An important issue concerning discrete photorefractive solitons is their ability to travel across the lattice at the so-called, transparent points associated with the vanishing of the well-known Peierls-Nabarro potential [15]. Although the systematic study of moving vector solitons is beyond the scope of the present work, even a simple-minded effort of setting the stationary pairs into transverse motion was partially successful. In particular, stationary solutions obtained by the Newton-Raphson algorithm, for the bright–bright soliton case, were multiplied by a transverse-momentum factor of the form $\exp(imn)$ (m being the relevant wave number), and input into the Runge-Kutta algorithm to examine their propagation dynamics. An example of such an attempt is shown in Fig. 7. The parameter values in this example are $\Lambda_1=\Lambda_2=-23.9$, $\beta=24.7$, and $m=0.3\pi$. Each component of the soliton pair has lost about 50% of its initial peak density at $z=100$, and then appears to reach a robust state (while still moving), since the peak densities maintain these values until at least $z=700$. This may be attributed to the recent findings associated with the existence of robust traveling waves in the context of the single-component photorefractive model in [24]. Clearly, this is a topic that merits further investigation (which, however, is outside the scope of the present work and will be left for future studies).

III. CONCLUSION

In this paper we have identified 14 species of two-component solitons in one-dimensional lattices with the saturable nonlinearity (both self-focusing and defocusing) that model arrays of photorefractive waveguides. In the experiment, the array can be induced by a deep photonic lattice. In the cases where both components of the soliton pair are of the same type, we have constructed families of asymmetric solutions, with equal propagation constants in both components. Soliton pairs of two types (both involving solely bright components) form entirely stable families, and four others build families that contain stable and unstable parametric regions. Additionally, eight other species are completely unstable. Five species of unstable pairs decay, while three others spontaneously evolve into their stable counterparts.

Noteworthy results were obtained for the vector-soliton families of the on-site dark–bright and on-site staggered-dark–staggered-bright "symbiotic" types, in the model with the self-defocusing and self-focusing sign of the nonlinearity, respectively. Both families contain stable parts. In the former

case, the in-phase bright component exists in the self-defocusing regime (where it cannot exist in isolation), due to the pairing to the dark component. Similarly, in the latter case, the stable on-site staggered-bright component, which would be impossible alone, is supported and stabilized by the coupling to the staggered-dark constituent of the vector soliton.

A brief effort to set the on-site bright–bright vector soliton in motion along the transverse dimension resulted in partial success. Each component of the soliton pair loses half of its peak density within 10 cm of propagation (along z), but then stabilizes and keeps traveling with these densities.

Stable soliton pairs predicted in this work can be implemented in the experiment using a strong photonic lattice in a photorefractive crystal. A scheme of the experiment and estimates of relevant parameters were given in the paper.

An interesting direction of extension of the present work would be to examine similar families of vector solitons in higher-dimensional settings. While such single-component studies have already been reported [25], their vector analogs will present a variety of interesting possibilities, including symbiotic structures, generalizing the one-dimensional ones presented herein. Such studies are currently in progress and will be reported in future publications.

[1] H. S. Eisenberg, Y. Silberberg, R. Morandotti, A. R. Boyd, and J. S. Aitchison, Phys. Rev. Lett. **81**, 3383 (1998).

[2] R. Morandotti, H. S. Eisenberg, Y. Silberberg, M. Sorel, and J. S. Aitchison, Phys. Rev. Lett. **86**, 3296 (2001).

[3] J. W. Fleischer, T. Carmon, M. Segev, N. K. Efremidis, and D. N. Christodoulides, Phys. Rev. Lett. **90**, 023902 (2003); D. Neshev, E. Ostrovskaya, Y. Kivshar, and W. Krolikowski, Opt. Lett. **28**, 710 (2003); J. W. Fleischer, M. Segev, N. K. Efremidis, and D. N. Christodoulides, Nature (London) **422**, 147 (2003); H. Martin, E. D. Eugenieva, Z. Chen, and D. N. Christodoulides, Phys. Rev. Lett. **92**, 123902 (2004).

[4] Y. S Kivshar, W. Krolikowski, and O. A. Chubykalo, Phys. Rev. E **50**, 5020 (1994).

[5] Y. S. Kivshar, Opt. Lett. **18**, 1147 (1993).

[6] J. W. Fleischer, G. Bartal, O. Cohen, T. Schwartz, O. Manela, B. Freedman, M. Segev, H. Buljan, and N. K. Efremidis, Opt. Express **13**, 1780 (2005).

[7] Z. Chen, H. Martin, E. D. Eugenieva, J. Xu, and J. Yang, Opt. Express **13**, 1816 (2005).

[8] N. K. Efremidis, S. Sears, D. N. Christodoulides, J. W. Fleischer, and M. Segev, Phys. Rev. E **66**, 046602 (2002).

[9] D. N. Christodoulides and R. I. Joseph, Opt. Lett. **13**, 794 (1988).

[10] D. N. Christodoulides, F. Lederer, and Y. Silberberg, Nature (London) **424**, 817 (2003).

[11] G. Stegeman and M. Segev, Science **286**, 1518 (1999).

[12] J. Meier, J. Hudock, D. Christodoulides, G. Stegeman, Y. Silberberg, R. Morandotti, and J. S. Aitchison, Phys. Rev. Lett. **91**, 143907 (2003).

[13] Z. Chen, A. Bezryadina, I. Makasyuk, and J. Yang, Opt. Lett. **29**, 1656 (2004).

[14] M. Stepić, D. Kip, L. Hadžievski, and A. Maluckov, Phys. Rev. E **69**, 066618 (2004); A. Khare, K. Ø. Rasmussen, M. R. Samuelsen, and A. Saxena, J. Phys. A **38**, 807 (2005).

[15] L. Hadžievski, A. Maluckov, M. Stepić, and D. Kip, Phys. Rev. Lett. **93**, 033901 (2004).

[16] J. Cuevas and J. C. Eilbeck, Phys. Lett. A **358**, 15 (2006).

[17] V. O. Vinetskii and N. V. Kukhtarev, Sov. Phys. Solid State **16**, 2414 (1975).

[18] M. Segev, G. C. Valley, B. Crosignani, P. DiPorto, and A. Yariv, Phys. Rev. Lett. **73**, 3211 (1994).

[19] D. N. Christodoulides, S. R. Singh, M. I. Carvalho, and M. Segev, Appl. Phys. Lett. **68**, 1763 (1996).

[20] J. W. Goodman, *Introduction to Fourier Optics*, 2nd ed. (McGraw-Hill, New York, 1996).

[21] P. G. Kevrekidis, H. Susanto, R. Carretero-Gonzalez, B. A. Malomed, and D. J. Frantzeskakis, Phys. Rev. E **72**, 066604 (2005).

[22] Y. S. Kivshar, D. Anderson, A. Hook, M. Lisak, A. A. Afanasjev, and V. N. Serkin, Phys. Scr. **44**, 195 (1991); S. C. Tsang, K. Nakkeeran, B. A. Malomed, and K. W. Chow, Opt. Commun. **249**, 117 (2005); V. M. Pérez-García and J. B. Beitia, Phys. Rev. A **72**, 033620 (2005); A. Gubeskys, B. A. Malomed, and I. M. Merhasin, *ibid.* **73**, 023607 (2006).

[23] Z. Chen, M. Segev, T. H. Coskun, D. N. Christodoulides, and Y. S. Kivshar, J. Opt. Soc. Am. B **14**, 3066 (1997).

[24] T. R. O. Melvin, A. R. Champneys, P. G. Kevrekidis, and J. Cuevas, nlin.PS/0603071.

[25] R. A. Vicencio and M. Johansson, Phys. Rev. E **73**, 046602 (2006).